Biomedical Signal Processing and Control 110 (2025) 108129

Contents lists available at ScienceDirect

Biomedical Signal Processing and Control

journal homepage: www.elsevier.com/locate/bspc

Effect of *MAPT* gene variations on the brain electrical activity: A multiplex network study

Aarón Maturana-Candelas [a,b,*], Roberto Hornero [a,b,c], Jesús Poza [a,b,c], Víctor Rodríguez-González [a,b], Víctor Gutiérrez-de Pablo [a,b], Nadia Pinto [d,e,f], Miguel A. Rebelo [d,g], Carlos Gómez [a,b]

[a] Biomedical Engineering Group, E.T.S.I. de Telecomunicación, Universidad de Valladolid, 47011, Valladolid, Spain
[b] Centro de Investigación Biomédica en Red en Bioingeniería, Biomateriales y Nanomedicina, (CIBER-BBN), Spain
[c] Instituto de Investigación en Matemáticas (IMUVA), Universidad de Valladolid, 47011, Valladolid, Spain
[d] Instituto de Investigacão e Inovacão em Saúde (I3S), Porto, Portugal
[e] Instituto de Patologia e Imunologia Molecular da Universidade do Porto (IPATIMUP), Universidade do Porto, Porto, Portugal
[f] Centro de Matemática da Universidade do Porto (CMUP), Porto, Portugal
[g] Faculdade de Ciências da Universidade do Porto (FCUP), Porto, Portugal

ARTICLE INFO

Keywords:
Alzheimer's disease
Electroencephalogram
Genetics
Tau
Brain connectivity
Microtubule-associated protein tau (*MAPT*)

ABSTRACT

The aim of this study is to examine how variations in the microtubule-associated protein tau (*MAPT*) gene affect the brain functional network. For this purpose, resting-state electroencephalogram (EEG) data from 155 participants were acquired. This database included healthy controls and Alzheimer's disease patients carrying seven *MAPT* alleles associated with risk or protective effects against neuropathologies or abnormal tau levels. To assess the impact of each genotype on brain function, a multiplex network analysis quantified the connectivity contribution of each brain region across multiple EEG frequency bands (delta, theta, alpha, and beta). To this end, brain functional connectivity was first calculated for each brain region and frequency band using the phase lag index (PLI) parameter. The PLI adjacency matrices in each frequency band corresponded to the layers conforming the multiplex network. Subsequently, the participation coefficient (*P*) was computed in each brain region to reflect node degree diversification among frequency bands. Carriers of risk and protective alleles exhibited distinct values of *P*, especially in the left default mode network in healthy controls. In addition, carriers of the risk alleles generally presented higher network disruptions. Finally, significant differences in node degree values were observed across SNPs in the theta and beta frequency bands. These results suggest that different *MAPT* variants may lead to diverse tau species that influence brain function, particularly in brain regions involved in information flow management in preclinical states. These insights may help understanding network disturbances caused by molecular factors.

1. Introduction

Tauopathies are a group of neurodegenerative disorders that are characterized by the abnormal accumulation of tau protein in the brain [1]. Tau is a critical component in stabilizing cytoskeletal microtubules, which are essential for maintaining the structure and function of neurons [1]. However, in tauopathies, tau protein becomes hyperphosphorylated, leading to its detachment from microtubules and the formation of abnormal intracellular aggregates known as neurofibrillary tangles (NFTs) [1]. These tangles are considered to disrupt the normal functioning of neurons and are one of the histological hallmarks of multiple neurodegenerative diseases, such as Alzheimer's disease (AD) [1]. Previous studies have suggested that tau alterations may contribute to AD pathology through multiple biological pathways [2,3], indicating the significance of tau in various physiological mechanisms beyond cytoskeletal stabilization. Moreover, NFTs have been observed to exhibit cytotoxic properties and are associated with atrophy [4], cortical neurodegeneration [4], and cognitive impairment [5].

Human tau is encoded by the microtubule-associated protein tau (*MAPT*) gene, which spans approximately 133.9 kb of nucleotide sequence on chromosome 17q21 [6]. This protein is expressed in six major isoforms, assembled by the alternative splicing of exons 2, 3, and 10 [7]. Depending on the inclusion or exclusion of exon 10, tau is composed of three (3R-tau) or four (4R-tau) microtubule-binding domains,

* Correspondence to: E.T.S.I. de Telecomunicación, Campus Miguel Delibes, Paseo Belén 15, 47011, Valladolid, Spain.
E-mail address: aaron.maturana@uva.es (A. Maturana-Candelas).

https://doi.org/10.1016/j.bspc.2025.108129
Received 13 November 2024; Received in revised form 12 May 2025; Accepted 24 May 2025
Available online 17 June 2025

and abnormal splicing has been associated with several tauopathies [6]. The sophisticated process of RNA splicing is catalyzed by genetic signals located mainly in intronic sequences [8]. Therefore, spontaneous mutations or genetic inheritance could potentially modify tau structure and behavior by altering the genetic information. Single-nucleotide polymorphisms (SNPs) are the most common form of genetic modifications, which are single-base changes in specific genetic loci [9]. The effects of SNPs on various diseases have been assessed through multiple genome-wide association studies. Previous research has found statistical associations between specific genotypes and neurodegeneration as well as changes in plasma tau levels [10–12]. Different variants of the *MAPT* gene have been linked to these disorders, suggesting that certain *MAPT* alleles may confer a higher risk or protective effect. Although the molecular mechanisms affected by specific base variations in the genetic code are diverse, individual gene changes have been proposed to exert pleiotropic effects that influence tau misfolding [13]. This insight implies that SNPs may have a significant impact on tau molecular properties, which could affect its aggregation capacity and lead to more profuse NFT formation.

NFTs are not only associated with physiological disturbances, but also exhibit specific spatial deposition patterns. These molecules have consistently revealed a hierarchical propagation across the AD brain [7]. Moreover, it has been discovered that NFTs and other tau species spread throughout the brain by prion-like transfer mechanisms [14], that occur more frequently in regions with higher synaptic density [15]. Consequently, neural populations that act as central sites in the brain connectome may assimilate higher concentrations of NFTs. In fact, this predisposition has been suggested in other studies, with the default mode network (DMN) identified as the common region for all NFT propagation patterns [16]. The DMN is a characteristic brain region particularly activated during resting state and displaying high centrality in the brain network [17]. Additionally, the DMN is considered a brain "hub" that manages high-level cognitive functions, such as emotional processing, self-referential mental activity, and the evocation of previous experiences [18]. From a connectivity standpoint, brain hubs are defined as regions functionally connected to multiple clusters or occupying central positions within a single functional cluster [19]. Hubs balance the integration of information from different sources and its segregation into multiple, specialized pathways [20].

Since hubs consist of central nodes in the brain connectome, these regions suffer increased vulnerability. Damage to these nodes causes severe alterations in the structural integrity of the functional network [21]. Neurodegeneration states such as AD have been associated with abnormal DMN activation [22–24]. For this reason, obtaining information from cortical network functioning is crucial. Fortunately, brain functional connectivity can be studied by means of a relatively simple technique called electroencephalography (EEG). EEG captures spontaneous electrical activity in the cortex by measuring the synchronized fluctuations of pyramidal neurons using a set of electrodes placed on the scalp. Due to its high temporal resolution, EEG is sensitive to rapid and transient changes in neural rhythms, making it useful for assessing relationships between multiple brain oscillators. EEG is commonly used in the study of neurological disorders because of its low cost, portability, and non-invasiveness, and has been shown to be useful in detecting abnormalities in physiological patterns [25–27].

Some of the most notable changes of the EEG in AD are the shift of spectral power to slower frequency bands [28], lower entropy and complexity [29], and alterations in functional connectivity [30–32]. This last point is particularly important since it describes communications between different brain systems. Metrics such as amplitude envelope correlation [33], coherence [34], phase locking value [35], and phase lag index (PLI) [36] are used to study the connectivity between pairs of nodes. The latter two metrics are based on the relationship between the instantaneous phase properties from two sequences, which contain useful information to characterize changes in the brain functional network in pathological or stimulatory conditions [37–39]. For this reason, phase-derived metrics are suitable to study anomalies in diverse network properties calculated through graph theory parameters. On the other hand, graph parameters such as small-world features [40–42], path length [36,43,44], and clustering coefficient [45] are used to characterize AD-induced perturbations in the brain connectome. These observations suggest that the brain functional organization in AD is shaped towards more randomized, less efficient network configurations. In fact, AD has been even conceived as a "disconnection syndrome" in terms of functional and structural connectivity [46], also transcending into molecular disruptions resulting in selective hub vulnerability [47]. However, the interactions between multiple frequency bands are often neglected despite their importance in high-level cognitive processes [48–50]. Multiplex network analysis (MNA) is a novel technique that allows evaluating the integration of connectivity patterns across different frequency bands, enabling the assessment of nodal interactions through inter-layer coupling [51,52]. This technique demonstrated that functional networks activating in diverse frequency bands do not act as independent entities but rather in a more integrated manner [52]. MNA has been used to identify selective disruptions of hub regions in neurodegenerative states and cognitive disorders [51,53–57], providing useful evidence for understanding pathological mechanisms.

Since MNA has proven its ability to characterize relevant features of functional neural networks, it can be used to investigate how clinical factors, such as genetic features, could contribute to brain connectivity alterations. Based on this, we hypothesize that *MAPT* genotypes associated with neurodegeneration or tau anomalies may have an impact on brain electrical activity, particularly in regions located in the most active functional networks during resting-state. These changes would manifest as disruptions in the hub capacity across the brain, depending on the contribution of each region to the structure of the functional network. Thus, we aim to analyze the inter-layer properties of the brain functional connectivity between various *MAPT* variants to evaluate the impact of genetic sequencing on brain dynamics. To accomplish this, we propose applying MNA to EEG data from healthy control (HC) subjects and AD patients carrying risk and protective alleles of multiple SNPs located in *MAPT*. We anticipate that variations that are consistent among SNPs will be more closely related to tau properties and their effects on neurophysiology than to other aspects. To the best of our knowledge, no other study has used MNA to characterize the impact of several variants of the same gene on the brain functional network. As a result, this study combines advanced computational techniques with biological information to elucidate neurophysiological changes, which reflects a remarkable level of novelty. This manuscript is organized as follows: First, the "Materials and methods" section describes in detail the characteristics of the used database, the genetic analysis and selection criteria, and the stages of EEG processing and analysis. The "Results" section presents the findings obtained using the proposed methodology. Subsequently, the "Discussion" section offers physiological interpretations of the MNA alterations associated with the examined genetic variants. Finally, the "Conclusions" section is devoted to summarizing the main contributions of this work.

2. Materials and methods

2.1. Subjects

This study enrolled 155 elderly participants, who were classified in two groups: HC subjects (n = 45) and AD patients (n = 110). The latter were diagnosed according to the National Institute on Aging – Alzheimer's Association (NIA-AA) criteria [58]. Participants with specific clinical conditions, such as recent surgery, vascular pathology, hypercatabolic states, clinical history of neoplasia (active or under treatment), and chronic alcoholism were excluded. AD patients with atypical signs of disease progression were also excluded to minimize

Table 1
Demographic and genetic data. $\bar{x}$, average; SD, standard deviation; Ref, reference allele; Alt, altered allele; M, male; F, female; MMSE, Mini-Mental State Examination score; Eff, effect of the allele; R, risk allele; P, protective allele; HC, healthy control subjects; AD, Alzheimer's disease patients; In, intronic variant; Ex, exonic variant; 3'UTR, 3' untranslated region; A, adenine; T, thymine; C, cytosine; G, guanine.

SNP	Base	Eff	Subjects		Sex (M:F)		Age ($\bar{x} \pm$ SD) (yrs.)		MMSE ($\bar{x} \pm$ SD)	
			HC	AD	HC	AD	HC	AD	HC	AD
rs2258689 (In/Ex)[a]	T (Ref)	P	27	75	14:13	40:35	80.0 ± 7.4	79.9 ± 7.5	28.9 ± 1.1	16.0 ± 7.6
	C (Alt)	R	18	35	8:10	20:15	79.2 ± 7.2	82.0 ± 6.6	28.8 ± 1.2	13.3 ± 8.2
rs242557 (In)	G (Ref)	P	18	44	8:10	22:22	81.3 ± 8.1	79.1 ± 7.2	28.8 ± 1.2	14.4 ± 8.3
	A (Alt)	R	27	66	14:13	35:31	78.7 ± 6.6	81.6 ± 7.2	28.9 ± 1.1	15.6 ± 7.6
rs11656151 (In)	A (Ref)	P	33	76	17:16	40:36	80.6 ± 8.0	80.8 ± 7.2	28.6 ± 1.1	15.3 ± 7.6
	G (Alt)	R	12	34	6:6	20:14	77.3 ± 4.3	80.1 ± 7.4	29.5 ± 0.7	14.6 ± 8.5
rs2435207 (In)	G (Ref)	P	20	52	9:11	25:27	80.4 ± 7.9	80.4 ± 6.3	29.1 ± 1.1	13.3 ± 8.3
	A (Alt)	R	25	58	14:11	30:28	79.2 ± 6.9	80.7 ± 8.1	28.7 ± 1.1	16.7 ± 7.2
rs16940758 (In)	C (Ref)	P	31	69	16:15	37:32	80.1 ± 6.9	80.6 ± 7.3	29.1 ± 1.0	14.3 ± 8.1
	T (Alt)	R	14	41	8:6	23:18	78.9 ± 8.2	80.6 ± 7.2	28.4 ± 1.2	16.4 ± 7.4
rs7521 (3'UTR)	C (Ref)	P	17	41	8:9	22:19	82.0 ± 8.4	80.0 ± 7.3	28.6 ± 1.2	16.2 ± 8.0
	A (Alt)	R	28	69	15:13	37:32	78.3 ± 6.3	80.9 ± 7.3	29.0 ± 1.1	14.5 ± 7.8
rs8070723 (In)	A (Ref)	R	23	62	12:11	34:28	77.7 ± 6.2	81.1 ± 7.0	28.7 ± 1.2	15.7 ± 7.5
	G (Alt)	P	22	48	11:11	24:24	81.8 ± 7.8	79.8 ± 7.6	29.0 ± 1.0	14.4 ± 8.4

[a] rs2258689 belongs to exon 6 or to an intron depending on the splicing process.

bias against other forms of dementia. The assessment of the cognitive state was carried out by means of the Mini-Mental State Examination (MMSE) test [59]. Each participant, relative, or legal representative provided informed consent, according to the recommendations of the Code of Ethics of the World Medical Association. This study was conducted in compliance with the Declaration of Helsinki and its protocol was approved by the Ethics Committee of the University of Porto (Porto, Portugal, Report nº 38/CEUP/2018).

2.2. Genetic analysis

In this study, biological material for genetic characterization was obtained from each subject through either a sample of saliva or buccal mucosa. Saliva samples (2 ml) were preferred and collected using the Oragene DNA 500 collection kit (DNAgenotek). For patients at advanced stages of the disease unable to voluntarily spit, we obtained buccal mucosa by means of three buccal swabs as an alternative. DNA extraction and quality control assessments were performed on all samples prior to analysis with the genome-wide Axiom Spain Biobank Array (Thermo Fisher Scientific) at the Spanish National Center for Genotyping (CEGEN). Variant calling quality control (QC) procedures were developed for both individuals and markers, according to Affymetrix best practices guide [60]. All analyses were performed using either Affymetrix Power Tools or PLINK [61]. Variants of the probes belonging to the recommended calling categories were annotated accordingly to the Genome Reference Consortium Human Build 37 (GRCh37) SNP assembly. Individual QC analyses were performed considering the sex of the individuals, duplications or relatedness, as well as divergent ancestry. In per-marker QC analysis, deviation from Hardy-Weinberg equilibrium and missingness rates were assessed.

Previous studies have shown significant associations between *MAPT* polymorphisms and neuropathologies or alterations in phosphorylated and total tau presence in cerebrospinal fluid (CSF). Matching them with those available in our database, the following 11 SNPs were selected: rs2258689 [62], rs242557 [63,64], rs11656151 [11], rs2435207 [62, 65], rs16940758 [66], rs7521 [67], rs8070723 [68], rs242562 [62, 65], rs1052553 [69], rs62063857 [69], and rs9468 [11]. A linkage disequilibrium (LD) test was conducted to assure no significant associations between these polymorphisms, resorting to the informatics tool LDlink [70], hosted by the Division of Cancer Epidemiology and Genetics site (National Institutes of Health, https://ldlink.nci.nih.gov; accessed February 15, 2023). The latter four SNPs (rs242562, rs1052553, rs62063857, and rs9468) showed high correlation values with other SNPs and were therefore disregarded to avoid redundant information. The remaining seven SNPs (rs2258689, rs242557, rs11656151, rs2435207, rs16940758, rs7521, and rs8070723) showed pairwise R2 values lower than 0.25 and were selected for further analysis. Heterozygotic and homozygotic subjects with altered alleles were classified in the same class. The SNPs rs242557, rs11656151, rs2435207, rs16940758, and rs8070723 were designated as variants in intronic loci; rs7521 was assigned as a variant in the 3' untranslated region (3'UTR); and rs2258689 is located at an intron or an exon depending on the splicing process according to GRCh37 patch release 13 (consulted at National Institutes of Health, https://www.ncbi.nlm.nih.gov; accessed February 20, 2023). Genetic and demographic data regarding each SNP are displayed in Table 1.

2.3. EEG recordings and pre-processing

For each subject, a 5-min EEG recording was acquired with a sampling frequency of 500 Hz and common average reference using a 19-channel Nihon Kohden Neurofax JE-921A EEG system. Electrodes were placed according to the international 10–20 system at Fp1, Fp2, F3, F4, F7, F8, T3, T4, T5, T6, C3, C4, P3, P4, O1, O2, Fz, Cz, and Pz. EEG recordings were obtained under resting-state conditions with closed eyes in a relaxed and noise-free environment. The skin impedance was attempted not to exceed 5 kΩ in each channel. The researchers controlled the state of vigilance of each subject to minimize drowsiness. The resulting data were stored in ASCII format on a personal computer.

Next, the EEG signals were pre-processed using a series of steps [71–73]: (i) mean removal; (ii) 1–30 Hz Hamming-window band-pass finite impulse response (FIR) filter, order 1000; (iii) removal of noise caused by electrode impedance and other biosignals using independent component analysis; (iv) signal segmentation into 5-s epochs, which provides a trade-off between stable statistical estimations and reliable feature extraction; (v) visual inspection of the signal and rejection of epochs contaminated with artifacts. The average number of artifact-free epochs among all subjects was 39.95 ± 12.74 (mean ± standard deviation, SD).

Once the EEG data were pre-processed, source-level signals were estimated using the standardized low resolution brain electromagnetic tomography (sLORETA) algorithm [74]. This algorithm estimates the distribution of electrical activity by maximizing the correlation between neighboring sources. Noise covariance was established as an identity matrix since no noise information was available. Noteworthy, this transformation may introduce bias in the calculation of the source-level activity if an atlas with higher number of sources than electrodes is used. For this reason, the Yeo-7 Network altas [75] with 14 regions of interest (ROIs) was proposed (7 ROIs in each hemisphere). This atlas defines each ROI according to distinct connectivity profiles from local networks named as: (i) visual network, (ii) somatomotor network, (iii) dorsal attention network, (iv) ventral attention network, (v) limbic

network, (vi) frontoparietal network, and (vii) DMN [75]. The EEG processing and pre-processing were performed digitally with MATLAB® (R2021b version, Mathworks, Natick, MA).

2.4. EEG analysis

First, the connectivity between each pair of ROIs was estimated from source-level EEG at each frequency layer. In this study, each layer corresponded to the classical frequency bands, defined as delta (δ, 1–4 Hz), theta (θ, 4–8 Hz), alpha (α, 8–13 Hz), and beta (β, 13–30 Hz). When calculating connectivity, it is important to consider primary and secondary leakage as they can lead to spurious estimations [76,77]. To address this issue, PLI was used since it is relatively insensitive to the effects of volume conduction [36,78]. PLI measures the asymmetry of the distributions of instantaneous phase differences between two time series [36], and it is defined as follows:

$$PLI = |\langle sign[sin(\Delta\phi(t_k))]\rangle|, \tag{1}$$

where $\Delta\phi(t_k)$ is the phase difference for each sample between two signals and $\langle\cdot\rangle$ indicates the mean value [36]. The resulting PLI values range between 0 and 1, with 0 denoting lack of coupling or a phase difference centered in zero (or π), and 1 a perfect, non-zero-centered, phase locking [36]. PLI was computed for each epoch, frequency band, and subject. Each PLI calculation resulted in a 14 × 14 adjacency matrix, representing pairwise connections between every ROI within the brain. This matrix captures the functional connectivity strength between different ROIs, indicating the degree of synchronization or correlation in neural activity. Finally, the average of all adjacency matrices of all the epochs at each frequency band was calculated; therefore, 4 matrices (*i.e.*, frequency layers), were assigned for each subject. The integration of these layers, consisting of the PLI-based functional connectivity between each pair of ROIs at each frequency band, yielded the multiplex network. In this study, the analysis focused on the relationships between each single node and the remaining nodes of its own layer, as well as itself in other layers, without considering inter-layer connections between different nodes [51,52,57].

In order to reveal multiplex features of specific nodes in a network, the calculation of the participation coefficient (P) was proposed. P quantifies the heterogeneity of the connectivity contribution of a node to the different communities of a network [79]. In this case, each community refers to each layer of the multiplex network. In other words, P allows to determine to what extent a node allocates its connectivity links to either a single layer or multiple layers homogeneously. P has previously been used to assess hub disruption in AD [53,57], aiding in characterizing the network alterations caused by the disease. To obtain this parameter, the degree of the node i on a layer ψ must first be computed [57,79]:

$$s_i^{[\psi]} = \sum_{j=1}^{n} w_{ij}^{[\psi]}, \qquad \psi = \{\delta, \theta, \alpha, \beta\}, \tag{2}$$

where w_{ij} is the PLI value between node i and j, and $n = 14$ is the number of nodes. Each layer (defined as ψ) corresponds to the PLI network obtained from the source-level signals filtered at each frequency band. Subsequently, the overlapped weighted degree was calculated as the sum of the PLI values between a node and its neighbors across layers. The overlapped weighted degree for the node i is

$$o_i = \sum_{\psi} s_i^{[\psi]}, \qquad \psi = \{\delta, \theta, \alpha, \beta\}. \tag{3}$$

The overlapped weighted degree was computed for each node resulting in 14 values for each subject. Finally, the value of the P coefficient associated with the node i was calculated as follows [57,79]:

$$P_i = \frac{M}{M-1}\left[1 - \sum_{\psi}\left(\frac{s_i^{[\psi]}}{o_i}\right)^2\right], \qquad \psi = \{\delta, \theta, \alpha, \beta\}, \tag{4}$$

where $M = 4$ is the number of layers. P values are ranged between 0 and 1. $P = 0$ indicates that connections between i and the rest of nodes lie in a single layer, whilst $P = 1$ corresponds to a perfectly homogeneous distribution of connectivity across all the layers [79]. To provide a clearer understanding, Fig. 1 illustrates the methodological process carried out to compute P. Subsequently, the obtained values of P coefficient in each ROI were categorized as risk-related or protective-related values depending on whether the subject was listed as carrying risk or protective alleles for each SNP. Finally, the grand average of the P values by subjects is calculated, yielding two values for each ROI and SNP: the risk- and the protective-related values. This process was conducted for both groups: HC subjects and AD patients.

After quantifying the heterogeneity of the connectivity contribution of each node with the P coefficient, the hub disruption was evaluated by means of the hub disruption index (k), proposed by Achard and colleagues [80]. The k parameter reflects the gradient of the regression line (least-squares first-order polynomial fit) that fits the P values of AD patients minus the average of the P values among HC subjects *vs.* the mean from the HC subjects. Values of k close to zero would imply similar impact exerted by genotypes in both healthy and pathological conditions, since variations of P in healthy subjects would be associated with equivalent variations in AD patients. Therefore, the k parameter allows to compare hub properties of a functional network between different groups. In this study, this process was repeated for each genetic variant of each SNP, and the results were displayed in a scatter-plot. The y-axis values in the chart represent P disruption, which we have defined as the difference between P values from AD patients and HC subjects [57]. Each SNP was represented by two sets of 14 ROIs, one for the risk allele and one for the protective allele populations. This representation allowed visual comparison of the differences between HC subjects and AD patients among different genotypes. Finally, the degree values of the nodes were analyzed in each layer individually, enabling a comparison of changes in functional connectivity between genotypes within each frequency band. This last step was conducted by calculating the node degree for each ROI within every layer. This parameter provides an absolute view of "gross" connectivity associated with each brain region and frequency band. Together with the P coefficient, which estimates the uniformity of connectivity value distribution across layers, both metrics allow a more exhaustive inspection of the multiplex network configuration. The methodological approach previously described represents an innovative application of MNA to elucidate alterations in the brain functional network, as the P coefficient and the node degree in each layer are used simultaneously to characterize the effects of various *MAPT* variations on cortical activation.

2.5. Statistical analysis

The Kolmogorov–Smirnov and Levene tests were performed to evaluate the normality and homoscedasticity of P and node degree values. Neither of these parameters met parametric assumptions. Thus, statistically significant differences between genotypes were identified using the non-parametric Mann–Whitney U-test ($\alpha = 0.05$). Additionally, multiple comparisons problem was dealt by means of false discovering rate (FDR) controlling procedure [81].

3. Results

In this study, the P coefficient was calculated from EEG data of HC subjects and AD patients. This metric was then used to determine differences in connectivity between subjects with risk and protective alleles in seven genetic *MAPT* loci. First, the hub disruption scatterplot was displayed in Fig. 2, where each point represents the P disruption value (*i.e.*, P in AD minus P in HC) *vs.* the average P value in HC subjects across ROIs. Protective allele carriers generally had lower P disruption values than risk allele carriers, with the former exhibiting

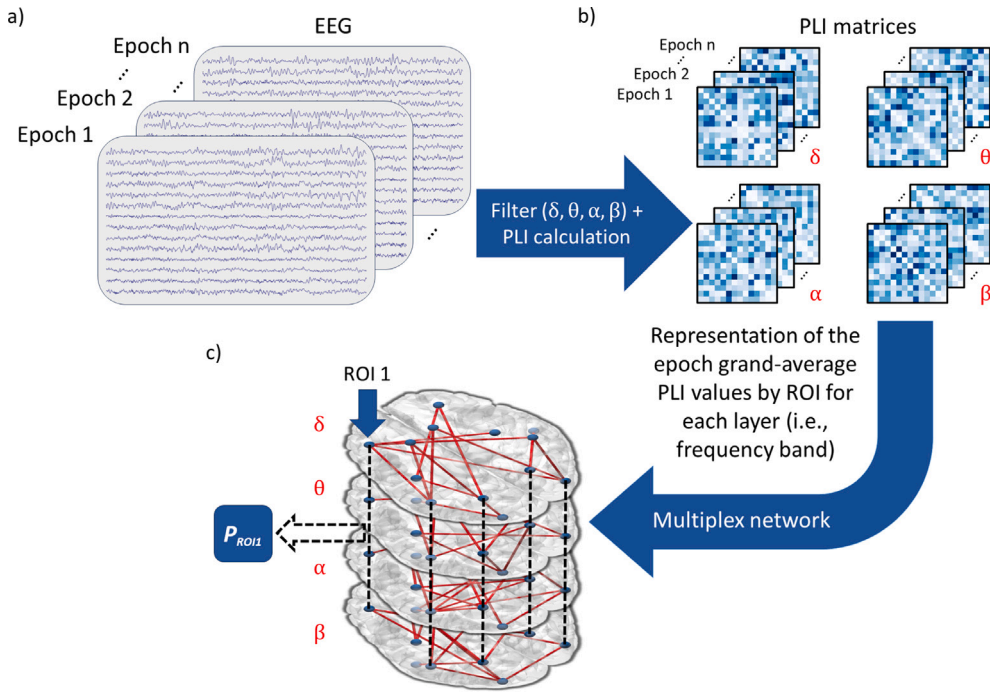

Fig. 1. Processing pipeline used to compute the participation coefficient (P): (a) The process begins with the segmentation of the 14-source EEG data into 5-s epochs, which have been pre-filtered in each frequency band; (b) Then the PLI matrices (14 × 14 size) are calculated for each epoch; subsequently, all the PLI matrices are averaged by epochs, resulting in a single 14 × 14 matrix for each frequency band; (c) Finally, the multiplex network is built from the four grand-averaged matrices (delta, theta, alpha, and beta), from which a value of P per ROI is calculated.

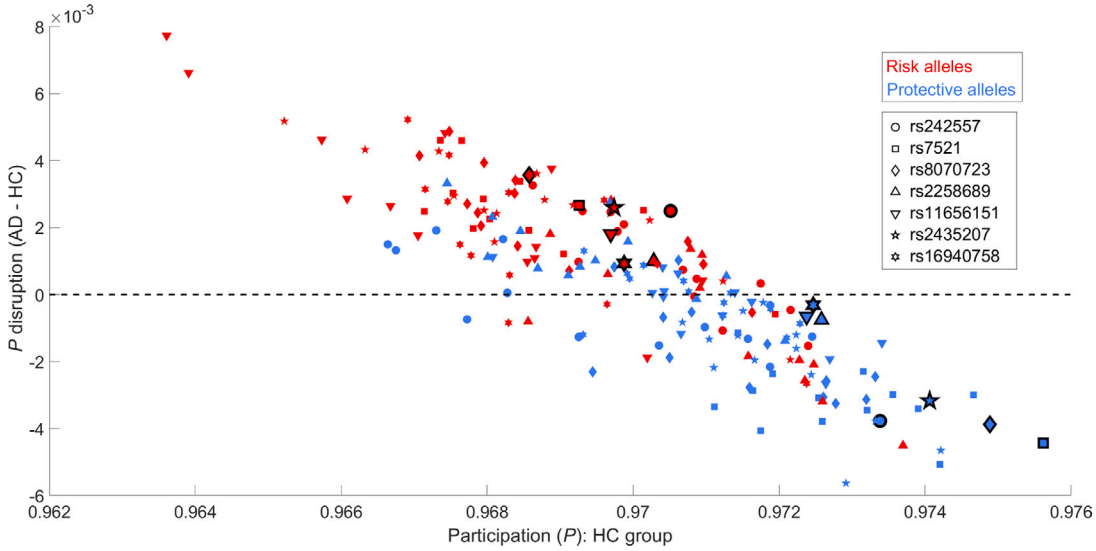

Fig. 2. Scatterplot of P disruption values *vs.* P values obtained from the HC group. Each symbol corresponds to an SNP. The symbols related to each SNP are as follows: circle for rs242557, square for rs7521, diamond for rs8070723, upward-pointing triangle for rs2258689, downward-pointing triangle for rs11656151, pentagram for rs2435207, and hexagram for rs16940758. Symbols with a black border represent the left DMN region. Red and blue colors display risk and protective alleles, respectively. The black dashed line indicates the zero crossing.

a grand average of -0.0010 ± 0.0015 and the latter showing a grand average of 0.0018 ± 0.0012 (mean ± SD). Noteworthy, a quick inspection of Fig. 2 reveals some SNPs whose protective alleles are related to the lowest values of P disruption averaged by ROIs, which are rs7521 ($-0.0032 \pm 9.688 \cdot 10^{-4}$), rs8070723 ($-0.0019 \pm 0.0015$), and rs2435207 ($-0.0022 \pm 0.0016$). In addition, these SNPs showed the highest values of the P coefficient averaged by ROIs in HC subjects for these alleles (0.9729 ± 0.0013, 0.9717 ± 0.0016, and 0.9722 ± 0.0011, respectively). Particularly, the SNP rs7521 presented the highest value of P coefficient in the controls' left DMN (0.9756).

Differences in P disruption values between genotypes may be due to three causes: (i) different connectivity patterns in controls, (ii) different connectivity patterns in AD patients, or (iii) both. To solve this question, the distribution of the P values in each SNP and genotype was obtained (Fig. 3). In the HC group, five of the seven SNPs reported significantly higher values of P in the protective alleles than in the risk alleles (rs7521, rs8070723, rs11656151, rs2435207, and rs16940758),

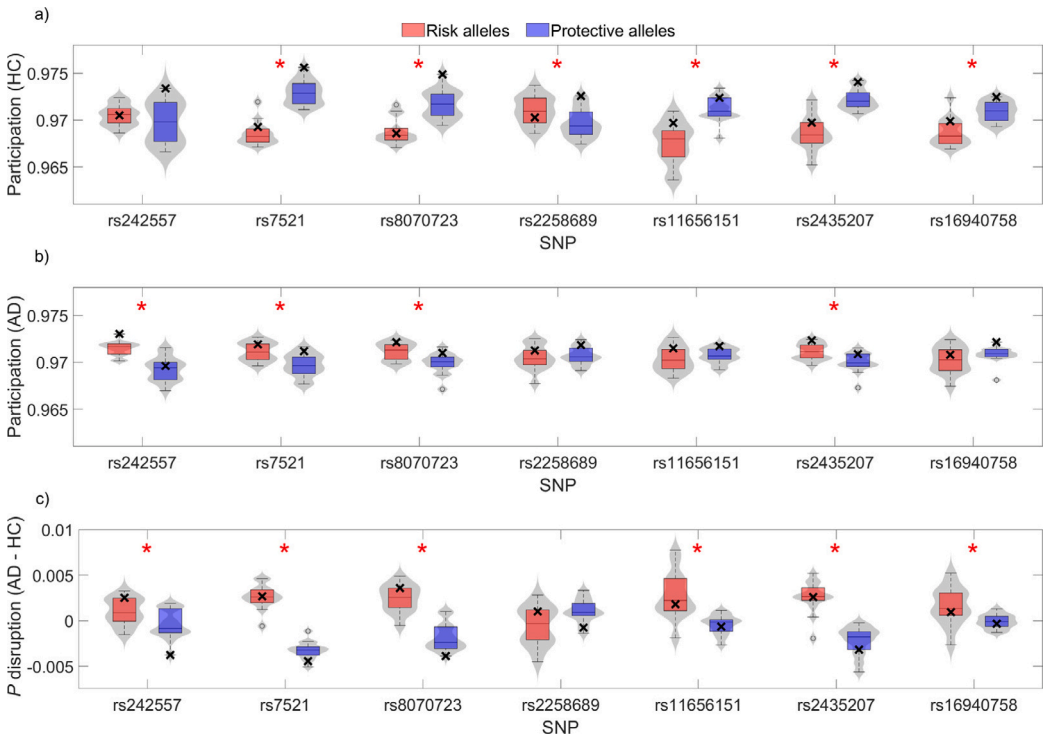

Fig. 3. Average *P* distribution between genotypes for all ROIs in (a) HC group and (b) AD group for each SNP. Also, *P* disruption values were displayed in (c). Statistically significant differences between genotypes were indicated with a red asterisk (*p*-values < 0.05, Mann–Whitney *U*-test with FDR correction). A black cross in each distribution indicates the value in the left DMN region.

one SNP showed the opposite relation (rs2258689), and one SNP did not show statistically significant differences between both subgroups (rs242557). In the AD group, significantly higher *P* values were obtained in the risk group in four SNPs (rs242557, rs7521, rs8070723, and rs2435207). The rest of the SNPs showed no statistically significant differences. These results suggest that different connectivity patterns in both HC subjects and AD patients contribute to the discrepancy in *P* disruption values between genotypes, as can also be observed in Fig. 3c. Fig. 3 also displayed the *P* and *P* disruption values regarding the left DMN (black crosses in each boxplot). This ROI was not only associated with the highest values of *P* in HC carriers of the protective alleles in most cases, but also with low values of *P* disruption (even the lowest in some SNPs). In fact, the absolute mean value of the *P* disruption across SNPs was highest in the left DMN ($4.6 \cdot 10^{-3}$). In addition, the left DMN exhibited higher *P* values in HC protective carriers in each SNP, with the highest mean across SNPs (0.974) in this allele. These observations suggest that this ROI is generally the most sensitive to genotype variations.

To evaluate the connectivity implications from each layer in the multiplex network, each frequency band was assessed individually. Theta and beta bands showed the most consistent trends in node degree between HC and AD patients, whilst delta and alpha bands exhibited more diverse patterns. Theta and beta band results were displayed in Fig. 4. In HC subjects, the protection allele group generally had lower node degree in the theta band, except for the SNPs rs2435207 and rs16940758. The opposite trend was observed in the beta band in all SNPs, except for rs11656151. In addition, AD patients showed generally lower and less consistent differences in node degree across all frequency bands.

Finally, the *P*-derived parameter *k* was obtained for each SNP and genotype from Fig. 2 and presented in Table 2. It is noteworthy that every SNP exhibited a negative value of *k*, which reflects an association between regions with high values of *P* in HC subjects and negative values of *P* disruption (*i.e.*, higher values of *P* in AD than HC). Also, significant differences were found between *k* values from risk and protective alleles (*p*-value = 0.011, Mann–Whitney *U*-test). This result indicates that ROIs with high *P* in a healthy brain functional network show more evident relative decreases of *P* in AD carriers of risk alleles.

Table 2
Hub disruption index (*k*) obtained from the gradient coefficient of the regression line from the *P* disruption scatterplot in each SNP. The statistical significance (Mann–Whitney *U*-test) of the differences between genotypes was also displayed.

SNP	k_{risk}	$k_{protect}$
rs242557	−1.112	−0.595
rs7521	−0.733	−0.352
rs8070723	−0.864	−0.704
rs2258689	−1.135	−0.660
rs11656151	−0.989	−0.628
rs2435207	−0.837	−0.108
rs16940758	−1.001	−0.402
Mean	**−0.953**	**−0.631**
***p*-value**	**0.011**	

4. Discussion

MNA of resting-state EEG activity was conducted for HC subjects and AD patients with different *MAPT* variants. Seven SNPs were studied in order to ascertain common alterations, which would be more likely to be associated with changes in the structural or biochemical properties of the tau protein.

4.1. Implications of *MAPT* variation on the global connectivity patterns

The *P* disruption values (*P* values in AD patients minus *P* values in HC subjects) were obtained for each SNP and ROI, and displayed in Fig. 2. Also, the *P* coefficient distribution across ROIs was expressed according to each SNP in Fig. 3. The analysis revealed that the *P* disruption values tended to be positive for risk alleles and negative for protective alleles. This observation suggests that the *P* coefficient in

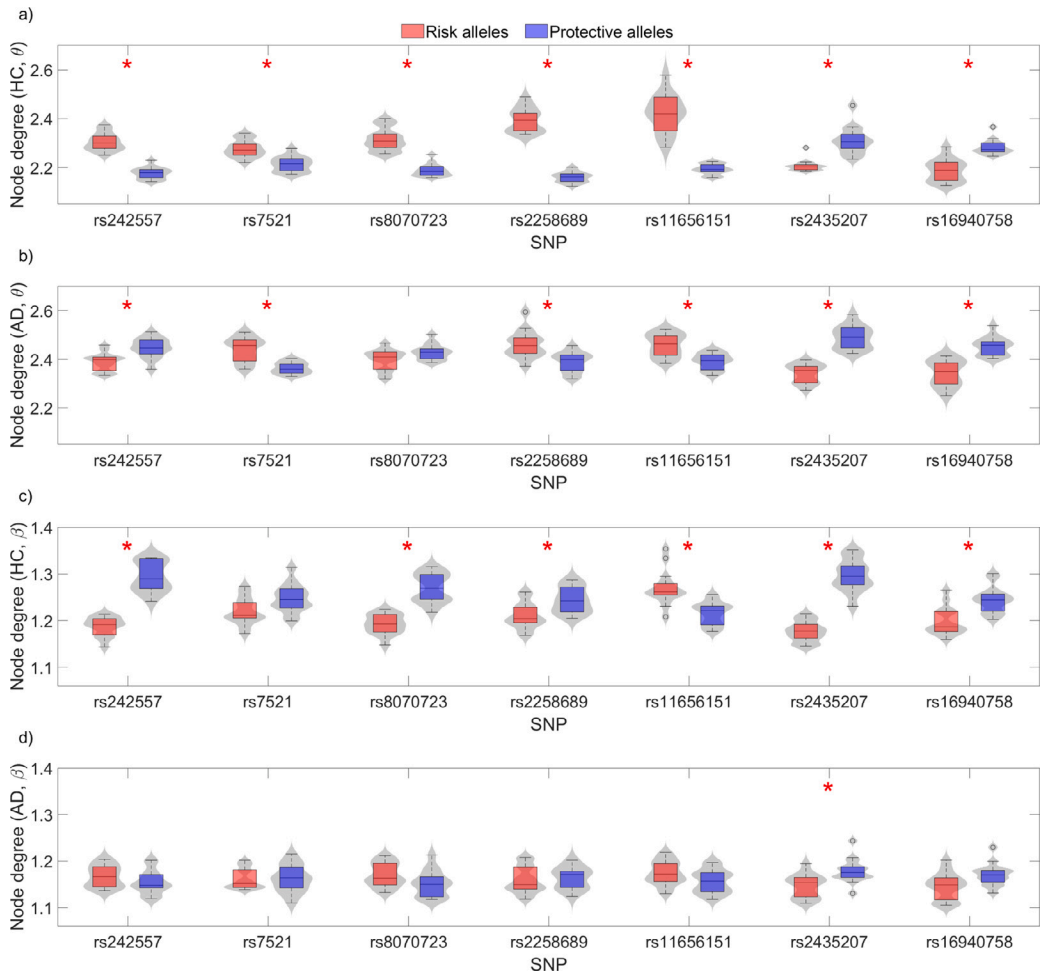

Fig. 4. Average node degree distribution in the theta and beta bands between subjects for all ROIs in each SNP: (a) HC group in theta band, (b) AD group in theta band, (c) HC group in beta band, and (d) AD group in beta band. Statistically significant differences between genotypes were indicated with a red asterisk (p-values < 0.05, Mann–Whitney U-test with FDR correction).

the AD group is higher in subjects with risk alleles compared to those with protective alleles, while the tendency is just the opposite for HC subjects. This disparity may arise due to the fact that the P coefficient in the AD group is significantly higher in subjects with risk alleles than in those with protective alleles, or that the P coefficient in the HC group is significantly higher in subjects with protective alleles than in those with risk alleles. At least, one of these premises is supported in every SNP, except in rs2258689, as it can be observed in Fig. 3. Moreover, the results of the analysis suggest that the effect of *MAPT* gene variations could differ depending on the clinical status. It was observed that different genotypes have a greater impact on the global network in healthy states, as shown in Fig. 3a, but milder effects in dementia states, as shown in Fig. 3b, resulting in an overall lower P disruption for protective groups, as shown in Fig. 3c. It is noteworthy that all SNPs of interest, except rs2258689, are located in non-coding regions, suggesting that these modifications are not related to translational processes that could directly affect the amino acid sequence. However, intronic variants have been previously linked to disruptions in splicing mechanisms that result in the inclusion of fragments of intronic code as pseudo-exons during mRNA maturation [82]. This phenomenon may lead to different tau isoforms that could have varied impacts, which may be more beneficial in preclinical stages but more detrimental in pathological stages. Since distinct sets of tau isoforms have been linked to different pathologies [6], it is plausible that structural changes could influence their cytotoxic behavior. Lastly, the SNPs rs7521, rs8070723, and rs2435207 reported the lowest P disruption values and the highest P coefficient values in controls. This observation implies that specific alterations to the tau protein hold a more pronounced influence on cerebral electrical activity, resulting in more evident deviations within the neural functional network. The SNP rs7521 was especially remarkable for the highest value of P coefficient associated with the left DMN in HC subjects. This finding could reflect the relation between some SNPs and physiological implications intimately related to maintaining healthy cognition or overall brain functioning. Previously, variations in rs7521 have been related to differences in 4R-tau expression, which contributes to altering the ratios between 4R and 3R tau [83]. In this way, the protective allele of rs7521 may play a crucial role in managing the balance of different tau isoforms with the aim of maintaining healthy ratios. This insight confirms that genetic variations do not affect physiological mechanisms in isolation, but rather interact in a non-linear and convoluted manner with other genetic features.

Furthermore, Table 2 displays the k coefficient for each SNP. This parameter reflects the impact of each genotype on the hub disruption of a network, which allows quantifying the loss of global ability of all the nodes to behave as hubs. The k values obtained from P in all SNPs showed statistically significant differences between genotypes. Also, the risk alleles were associated with lower values of k. This observation indicates that nodes that reported more homogeneous contributions across layers on the multiplex functional network in HC subjects exhibited less homogeneous contributions in AD patients when evaluating carriers of risk alleles. This insight suggests that the protective alleles of various SNPs could be generating a damping effect on the network disruptions, especially in hub regions.

4.2. Higher sensitivity to disruption and hub capacity in the left DMN region

The protective carriers subgroup of HC subjects shows the highest values of *P* in most of the SNPs, particularly in the left DMN region, as seen in Fig. 3a. Additionally, Fig. 3a reveals that HC subjects carrying protective alleles exhibit higher *P* coefficients in the left DMN than those with risk alleles, which indicates that the left DMN of HC subjects with protective alleles has greater inter-layer connectivity. This suggests that the protective allele helps to maintain the hub properties of the DMN when communicating with other brain regions during resting states, even in preclinical circumstances. Furthermore, the *P* disruption associated with the left DMN showed the lowest values in most cases (Fig. 3c) and was also negative in contrast to the risk genotype subgroups. Low *P* disruption values imply a more concentrated node contribution in a single layer. Therefore, we can infer that the left DMN of HC subjects carrying risk alleles may be associated with neuronal populations lacking the ability to integrate information from different layers, possibly due to their diminished hub capabilities.

As different frequency bands have been suggested to participate in brain functions at different spatio-temporal scales [84], lower values of *P* associated with HC carriers of risk alleles may indicate a slight deficit in functional specialization of the left DMN. Additionally, negative *P* disruption values in the left DMN could mean that this region is particularly sensitive to different isoforms of tau, altering its neural activity more significantly depending on the cytotoxic characteristics of this molecule. While only rs2258689 can be part of an exon during mRNA maturation, intronic variations are able to trigger alternative splicing processes. In fact, alternative splicing of pre-mRNAs is a major contributor to proteomic diversity [8]. Regarding AD groups, greater similarity between genotypes in patients may be due to the fact that the effect that tau may exert in neurodegenerative states is overshadowed by other physiological disruptions. Furthermore, the observed *P* fluctuations between ROIs could be a manifestation of compensatory mechanisms in specific brain regions in processes involving flow and management of neural information. Previously, this idea was proposed when obtaining an increase of *P* in frontal areas in AD [53]. In this sense, brain regions that are not typically acting as hubs could be adopting this role with the aim of maintaining the functional integrity of the network.

An anatomical explanation for the multiplex disruptions in the DMN is demyelination. Histological examinations have shown a correlation between the spread of AD pathology and the reversed myelination process during brain development [85]. Since this propagation is similar to NFT deposition along the AD continuum, these neuronal populations may be more resistant to the cytotoxic effects of hyperphosphorylated tau. In fact, a previous study has suggested a relationship between myelin and resistance against the detrimental effects of tau [86], which complements the finding of a robust association between decreased myelin and elevated tau concentrations [87]. Given the late myelination displayed by the DMN during brain development [88], these regions may be notably more sensitive to *MAPT* variability.

Another effect behind the obtained results is related to greater sensitivity of the DMN to tau cytotoxicity, which could be associated with a greater predisposition to accumulate elevated levels of this protein. NFTs and other tau by-products are known to spread between neuronal populations by means of prion-like transfer mechanisms [14], which are more likely to activate in regions of high synaptic density [15]. Recently, resting-state networks, such as the DMN, have reported increased synaptic density compared to other brain regions [89]. Since this feature reflects greater structural connection between diverse neural populations, the likelihood to collect higher concentrations of tau is expected to increase. Conversely, brain regions with lower synaptic density may be less affected not due to resistance to cytotoxicity, but simply because of lower protein presence. Typically, genetic variations in expression quantitative trait loci (eQTL, see [90]) have been associated with differences in transcript abundance. The SNP rs8070723 is the only one previously cataloged as an eQTL for the *MAPT* gene in the brain (p-value < 0.001, consulted at GTEx Portal v8, Broad Institute of MIT and Harvard, https://www.gtexportal.org; accessed February 21, 2023). However, alternative genetic traits associated with different protein concentrations have been suggested [12], implicating that not only eQTLs may cause alterations in genetic expression levels.

4.3. Consistent changes in specific frequency bands may be directly related with different tau species

After applying MNA to the EEG data, the contribution of each individual layer to the functional network was assessed. For this purpose, the node degree at each frequency band was obtained by averaging across subjects. This approach can identify which layers are most affected by genotype variations. Theta and beta bands showed mostly consistent results, which are presented in Fig. 4. The theta band has been widely studied in neurodegenerative processes, with multiple pieces of evidence linking alterations in theta activity to cognitive impairment [25]. Previous research examining brain activity disruptions has also reported a strong association between tau/amyloid ratios and an increase in relative theta activity in healthy subjects [91]. Additionally, evidence linking different tau species to the theta frequency band has been documented in mice models, suggesting that the sequence of tau can modulate the power of specific brain oscillations [92]. These insights could explain the alterations in node degree values found in the theta band between genotypes in the HC group. On the other hand, brain beta oscillations are also affected in the slowing of brain activity associated with neurodegeneration progression [25]. Again, further evidence has shown that abnormal tau levels are correlated with decreased functional connectivity [93] and global power [94] in fast frequencies. As different *MAPT* variants may be associated with an increase of tau levels [12], beta activity could also be affected by genetic variations. We suggest these mechanisms could be partially the reason for the consistent trends in beta and theta bands between genotypes obtained in this study.

4.4. Potential physiological repercussions of diverse tau configurations in the brain functional network

There are various potential explanations as to why different alleles of *MAPT* could be disrupting functional connectivity in the brain. Firstly, it is possible that these disruptions could be a result of the quantity of tau produced. It has been suggested that distinct *MAPT* alleles are associated with different concentrations of CSF tau in amyloid-positive individuals [95]. In fact, one of the studied SNPs (rs16940758) has been related with this alteration, although it was not the case for rs7521, rs242557, and rs2258689 [95]. However, it is plausible that the other selected SNPs could also have a similar impact. Furthermore, it is worth noting that different variants in *MAPT* may not necessarily be associated with increased tau synthesis, as certain isoforms may be more susceptible to degradation or removal from brain tissue than others. This may be related to the ubiquitin-proteasome system, which recognizes and degrades proteins with abnormal folding patterns [96].

Another potential explanation for the disruption of functional connectivity is the abnormal folding of tau. An earlier study suggested that alterations in tau folding can result in increased protein aggregations due to elevated tau-tau interactions [97]. While this study linked these abnormal folds to the presence of beta-amyloid, it is possible that tau configurations that affect its folding could lead to higher concentrations of this molecule and more intense cytotoxic and immunological responses.

In addition, multiple tau variants may have significant effects on their spreading pathways through the brain. A previous study reported evidence of heterogeneous tau pathology propagation resulting from different tau species [98]. This factor may be important in elucidating why certain SNPs are associated with more pronounced disruptions in

the DMN than others. This relationship can also be explained by the folding of tau, as evidence suggests that distinct structural configurations of tau are associated with different propagation patterns in the brain [99]. This supports the idea that changes in the primary structure of tau can lead to alterations in tau folding.

Finally, it is worth noting that different tau species may lead to a variety of physiological disruptions, such as reduced binding to microtubules resulting in decreased tubulin assembly [6]. Other sources have linked specific structural configurations with impaired functionality. For instance, paired helical filaments of tau were shown to be nearly incompetent in terms of microtubule assembly [100], demonstrating that the structure of tau can affect its physiological properties. Even small changes, such as the substitution of serine and threonine residues with glutamate, can have significant impact on tau cytotoxicity [101]. This point supports the idea that minimal alterations in the peptide chain of a protein can result in significant perturbations in cell function.

In order to minimize the damage derived from tau isoforms associated with disruptions in the brain connectome, tau-targeted therapies could be applied. These clinical approaches obtained promising results in detecting and removing specific tau species from the brain tissue. Immunotherapy is able to facilitate tau clearance from the brain to the periphery, as evidenced by increased tau concentrations in blood following immunization [102]. In addition, various tau species can be targeted, including amino- and carboxy-termini, proline-rich areas, and microtubule-binding domains [103]. Therefore, tau isoforms diverging from the wild variant in specific amino acids may be potentially targetable and removed in the near future. During the past years, clinical trials have been conducted to evaluate the safety and efficacy of tau-targeted immunotherapies in humans [103,104]. These applications show potential to diminish the impact of the most pathogenic tau species that could be trackable by genetic screenings.

4.5. Limitations and future research

While this study found significant associations between *MAPT* variants and changes in the brain functional network, some limitations are necessary to be pointed out. First and foremost, the study was conducted exclusively using EEG and genetic data, and as such, there is no direct evidence confirming the link between *MAPT* sequence and neurophysiological alterations. The factors proposed in this work relating to genotypes, tau properties, and EEG disruptions are not intended to describe causal relationships, but rather suggest a variety of possible implications that could explain the results obtained. To validate these associations, additional clinical data, such as medical imaging, would be required to determine tau-related alterations. Secondly, the participants were classified into genetic subgroups for each category, which resulted in relatively sparse sample sets, especially for the HC subgroups. This issue could lead to outliers and bias in the data provided by the MNA. For this reason, efforts directed towards obtaining larger datasets should be encouraged. Furthermore, our database consists in 19-channel EEG data, which is relatively lacking in spatial resolution. While we aimed to keep costs low for the sake of feasibility, our goal in future research is to gain access to more sophisticated means of acquisition. Increasing the spatial resolution would allow the use of more detailed atlases, thus providing more accurate information on specific brain regions. Finally, only SNPs were considered in this study, despite other polymorphisms, such as insertions or deletions, may also provide interesting insights when analyzing EEG alterations.

In future research, we plan to expand the methodological framework established in this study by incorporating additional perspectives. Specifically, we will examine a broader set of metrics derived from EEG signals, including spectral and nonlinear metrics, as well as graph theory parameters computed across multiple frequency bands. These features have been shown to capture anomalies resulting from both pathological and non-pathological brain perturbations [53,105].

5. Conclusions

This study analyzed resting-state EEG data from HC subjects and AD patients carrying risk and protective variants of *MAPT* against neurodegeneration or tau anomalies using MNA. The main contributions of this work are twofold. First, we proposed a relationship between hub behavior and alterations in MNA-derived parameters; and second, we identified genetically driven associations linking these two key aspects with tau potential anomalies. This insight may be related to the effects of different tau structural properties on the configuration of the brain functional network. The most evident differences in the left DMN between genotypes were observed in HC subjects, which indicates that the effect of genetic factors may be more prominent in preclinical states than in pathological ones. This could be due to the fact that the impact of alterations caused by different tau isoforms diminishes as the level of structural disruption increases. Additionally, this observation suggests that the detrimental effects of different tau species in the left DMN can influence brain electrical activity before any AD symptoms develop. However, further investigation is needed to fully understand the mechanisms that play a role in these disruptions.

CRediT authorship contribution statement

Aarón Maturana-Candelas: Writing – review & editing, Writing – original draft, Visualization, Resources, Methodology, Investigation, Formal analysis, Data curation, Conceptualization. **Roberto Hornero:** Writing – review & editing, Validation, Resources, Project administration, Conceptualization. **Jesús Poza:** Writing – review & editing, Validation, Conceptualization. **Víctor Rodríguez-González:** Writing – review & editing, Validation, Data curation. **Víctor Gutiérrez-de Pablo:** Writing – review & editing, Validation. **Nadia Pinto:** Writing – review & editing, Validation, Resources. **Miguel A. Rebelo:** Writing – review & editing, Validation. **Carlos Gómez:** Writing – review & editing, Validation.

Funding

This research has been developed under the grant PGC2018-098214 -A-I00 funded by “Ministerio de Ciencia e Innovación”/“Agencia Estatal de Investigación”/10.13039/501100011033 and by ‘European Regional Development Fund (ERDF) A way of making Europe’, by the ‘European Union’; under the R+D+i project “Análisis y correlación entre la epigenética y la actividad cerebral para evaluar el riesgo de migraña crónica y episódica en mujeres” (‘Cooperation Programme Interreg V-A Spain-Portugal POCTEP 2014–2020’) funded by ‘European Commission’ and ERDF; by “CIBER en Bioingeniería, Biomateriales y Nanomedicina (CIBER-BBN)” through “Instituto de Salud Carlos III (ISCIII)” co-funded with ERDF funds; under the grant PID2022-138286NB-I00 funded by “Ministerio de Ciencia e Innovación”/“Agencia Estatal de Investigación”/10.13039/501100011033 and by “ERDF A way of making Europe”; and by Portuguese funds through “FCT-Fundação para a Ciência e a Tecnologia”/“Ministério da Ciência, Tecnologia e Inovação” in the framework of the projects ‘Institute for Research and Innovation in Health Sciences’ (POCI-01–0145-FEDER-007274). A.M.-C. was in receipt of a PIF grant by the “Consejería de Educación de la Junta de Castilla y León”. V.R.-G. and V.G.-d.P. were in receipt of a PIF grant by the ‘University of Valladolid’. N.P. is supported by “FCT-Fundação para a Ciência e a Tecnologia”, under the program contract provided in Decree-Law no.57/2016 of August 29. The genotyping service was carried out at CEGEN-PRB3-ISCIII; it is supported by grant PT17/0019, of the PE I+D+i 2013–2016, funded by ISCIII and ERDF.

Declaration of competing interest

The authors declare that they have no known competing financial interests or personal relationships that could have appeared to influence the work reported in this paper.

Acknowledgments

We deeply thank all participants, families and institutions involved: Asociación de Familiares de Enfermos de Alzheimer de Ávila, Ávila; Associação de Pensionistas e Reformados de Viana do Castelo, Viana do Castelo; Casa do Povo de Alvito S.Pedro, Barcelos; Santa Casa da Misericórdia de Vila Nova de Gaia; Obra Social Nossa Senhora da Boa Viagem, Porto; Gero Vida, Villaralbo (Zamora); Asociación de Familiares de Alzheimer de León; Residencia San Raimundo en Coreses; Centro de Dia S. João de Deus, da Santa Casa da Misericórdia do Porto; Lar Santa Rita, da Santa Casa da Misericórdia de Caminha; Centro Social e Cultural de Vila Praia de Âncora; Lar Casa de Magalhães; Armonía Centro de Día, Zamora. Also, we want to express our gratitude to Patricia Sousa from 'Associação Portuguesa de Familiares e Amigos dos Doentes de Alzheimer' and Carmen Pita from 'Asociación de Familiares y Amigos de Enfermos de Alzheimer y Otras Demencias de Zamora'. They contributed with their psychological and caregiver skills to ease the stress of the patients.

Data availability

Data will be made available on request.

References

[1] H. Chi, T.-K. Sang, H.-Y. Chang, Tauopathy, 2019, http://dx.doi.org/10.5772/intechopen.73198.

[2] Q. Feng, Y. Luo, X.-N. Zhang, X.-F. Yang, X.-Y. Hong, D.-S. Sun, X.-C. Li, Y. Hu, X.-G. Li, J.-F. Zhang, X. Li, Y. Yang, Q. Wang, G.-P. Liu, J.-Z. Wang, MAPT/Tau accumulation represses autophagy flux by disrupting IST1-regulated ESCRT-III complex formation: a vicious cycle in Alzheimer neurodegeneration, Autophagy 16 (4) (2020) 641–658, http://dx.doi.org/10.1080/15548627.2019.1633862.

[3] S.A. Kent, T.L. Spires-Jones, C.S. Durrant, The physiological roles of tau and Aβ: implications for Alzheimer's disease pathology and therapeutics, Acta Neuropathol. 140 (4) (2020) 417–447, http://dx.doi.org/10.1007/s00401-020-02196-w.

[4] R. La Joie, A.V. Visani, S.L. Baker, J.A. Brown, V. Bourakova, J. Cha, K. Chaudhary, L. Edwards, L. Iaccarino, M. Janabi, O.H. Lesman-Segev, Z.A. Miller, D.C. Perry, J.P. O'Neil, J. Pham, J.C. Rojas, H.J. Rosen, W.W. Seeley, R.M. Tsai, B.L. Miller, W.J. Jagust, G.D. Rabinovici, Prospective longitudinal atrophy in Alzheimer's disease correlates with the intensity and topography of baseline tau-PET, Sci. Transl. Med. 12 (524) (2020) http://dx.doi.org/10.1126/scitranslmed.aau5732.

[5] A. Bejanin, D.R. Schonhaut, R. La Joie, J.H. Kramer, S.L. Baker, N. Sosa, N. Ayakta, A. Cantwell, M. Janabi, M. Lauriola, J.P. O'Neil, M.L. Gorno-Tempini, Z.A. Miller, H.J. Rosen, B.L. Miller, W.J. Jagust, G.D. Rabinovici, Tau pathology and neurodegeneration contribute to cognitive impairment in Alzheimer's disease, Brain 140 (12) (2017) 3286–3300, http://dx.doi.org/10.1093/brain/awx243.

[6] A. Corsi, C. Bombieri, M.T. Valenti, M.G. Romanelli, Tau isoforms: Gaining insight into MAPT alternative splicing, Int. J. Mol. Sci. 23 (23) (2022) 15383, http://dx.doi.org/10.3390/ijms232315383.

[7] S. Takeda, Progression of Alzheimer's disease, tau propagation, and its modifiable risk factors, Neurosci. Res. 141 (2019) 36–42, http://dx.doi.org/10.1016/j.neures.2018.08.005.

[8] Z. Wang, C.B. Burge, Splicing regulation: From a parts list of regulatory elements to an integrated splicing code, RNA 14 (5) (2008) 802–813, http://dx.doi.org/10.1261/rna.876308.

[9] T. Fadason, S. Farrow, S. Gokuladhas, E. Golovina, D. Nyaga, J.M. O'Sullivan, W. Schierding, Assigning function to SNPs: Considerations when interpreting genetic variation, Semin. Cell Dev. Biol. 121 (2022) 135–142, http://dx.doi.org/10.1016/j.semcdb.2021.08.008.

[10] M. Tábuas-Pereira, I. Santana, R. Guerreiro, J. Brás, Alzheimer's disease genetics: Review of novel loci associated with disease, Curr. Genet. Med. Rep. 8 (1) (2020) 1–16, http://dx.doi.org/10.1007/s40142-020-00182-y.

[11] A. Gerrish, G. Russo, A. Richards, V. Moskvina, D. Ivanov, D. Harold, R. Sims, R. Abraham, P. Hollingworth, J. Chapman, M. Hamshere, J.S. Pahwa, K. Dowzell, A. Williams, N. Jones, C. Thomas, A. Stretton, A.R. Morgan, S. Lovestone, J. Powell, P. Proitsi, M.K. Lupton, C. Brayne, D.C. Rubinsztein, M. Gill, B. Lawlor, A. Lynch, K. Morgan, K.S. Brown, P.A. Passmore, D. Craig, B. McGuinness, S. Todd, J.A. Johnston, C. Holmes, D. Mann, A.D. Smith, S. Love, P.G. Kehoe, J. Hardy, S. Mead, N. Fox, M. Rossor, J. Collinge, W. Maier, F. Jessen, H. Kölsch, R. Heun, B. Schürmann, H.V.D. Bussche, I. Heuser, J. Kornhuber, J. Wiltfang, M. Dichgans, L. Frölich, H. Hampel, M. Hüll, D. Rujescu, A.M. Goate, J.S.K. Kauwe, C. Cruchaga, P. Nowotny, J.C. Morris, K. Mayo, G. Livingston, N.J. Bass, H. Gurling, A. McQuillin, R. Gwilliam, P. Deloukas, G. Davies, S.E. Harris, J.M. Starr, I.J. Deary, A. Al-Chalabi, C.E. Shaw, M. Tsolaki, A.B. Singleton, R. Guerreiro, T.W. Mühleisen, M.M. Nöthen, S. Moebus, K.-H. Jöckel, N. Klopp, H.-E. Wichmann, M.M. Carrasquillo, V.S. Pankratz, S.G. Younkin, L. Jones, P.A. Holmans, M.C. O'Donovan, M.J. Owen, J. Williams, The role of variation at AβPP, PSEN1, PSEN2, and MAPT in late onset Alzheimer's disease, J. Alzheimer's Dis. 28 (2) (2012) 377–387, http://dx.doi.org/10.3233/JAD-2011-110824.

[12] J. Chen, J.-T. Yu, K. Wojta, H.-F. Wang, H. Zetterberg, K. Blennow, J.S. Yokoyama, M.W. Weiner, J.H. Kramer, H. Rosen, B.L. Miller, G. Coppola, A.L. Boxer, Genome-wide association study identifies MAPT locus influencing human plasma tau levels, Neurology 88 (7) (2017) 669–676, http://dx.doi.org/10.1212/WNL.0000000000003615.

[13] Y. Chornenkyy, D.W. Fardo, P.T. Nelson, Tau and TDP-43 proteinopathies: kindred pathologic cascades and genetic pleiotropy, Lab. Invest. 99 (7) (2019) 993–1007, http://dx.doi.org/10.1038/s41374-019-0196-y.

[14] A. Mudher, M. Colin, S. Dujardin, M. Medina, I. Dewachter, S.M. Alavi Naini, E.-M. Mandelkow, E. Mandelkow, L. Buée, M. Goedert, J.-P. Brion, What is the evidence that tau pathology spreads through prion-like propagation? Acta Neuropathol. Commun. 5 (1) (2017) 99, http://dx.doi.org/10.1186/s40478-017-0488-7.

[15] S. Calafate, A. Buist, K. Miskiewicz, V. Vijayan, G. Daneels, B. de Strooper, J. de Wit, P. Verstreken, D. Moechars, Synaptic contacts enhance cell-to-cell Tau pathology propagation, Cell Rep. 11 (8) (2015) 1176–1183, http://dx.doi.org/10.1016/j.celrep.2015.04.043.

[16] J.W. Vogel, A.L. Young, N.P. Oxtoby, R. Smith, R. Ossenkoppele, O.T. Strandberg, R. La Joie, L.M. Aksman, M.J. Grothe, Y. Iturria-Medina, M.J. Pontecorvo, M.D. Devous, G.D. Rabinovici, D.C. Alexander, C.H. Lyoo, A.C. Evans, O. Hansson, Four distinct trajectories of tau deposition identified in Alzheimer's disease, Nature Med. 27 (5) (2021) 871–881, http://dx.doi.org/10.1038/s41591-021-01309-6.

[17] K. Smitha, K. Akhil Raja, K. Arun, P. Rajesh, B. Thomas, T. Kapilamoorthy, C. Kesavadas, Resting state fMRI: A review on methods in resting state connectivity analysis and resting state networks, Neuroradiol. J. 30 (4) (2017) 305–317, http://dx.doi.org/10.1177/1971400917697342.

[18] M.E. Raichle, The brain's default mode network, Annu. Rev. Neurosci. 38 (1) (2015) 433–447, http://dx.doi.org/10.1146/annurev-neuro-071013-014030.

[19] C.J. Honey, R. Kötter, M. Breakspear, O. Sporns, Network structure of cerebral cortex shapes functional connectivity on multiple time scales, Proc. Natl. Acad. Sci. 104 (24) (2007) 10240–10245, http://dx.doi.org/10.1073/pnas.0701519104.

[20] R.L. Buckner, J. Sepulcre, T. Talukdar, F.M. Krienen, H. Liu, T. Hedden, J.R. Andrews-Hanna, R.A. Sperling, K.A. Johnson, Cortical Hubs revealed by intrinsic functional connectivity: Mapping, assessment of stability, and relation to Alzheimer's disease, J. Neurosci. 29 (6) (2009) 1860–1873, http://dx.doi.org/10.1523/JNEUROSCI.5062-08.2009.

[21] X. Wang, Q. Lin, M. Xia, Y. He, Differentially categorized structural brain hubs are involved in different microstructural, functional, and cognitive characteristics and contribute to individual identification, Hum. Brain Mapp. 39 (4) (2018) 1647–1663, http://dx.doi.org/10.1002/hbm.23941.

[22] D.T. Jones, M.M. Machulda, P. Vemuri, E.M. McDade, G. Zeng, M.L. Senjem, J.L. Gunter, S.A. Przybelski, R.T. Avula, D.S. Knopman, B.F. Boeve, R.C. Petersen, C.R. Jack, Age-related changes in the default mode network are more advanced in Alzheimer disease, Neurology 77 (16) (2011) 1524–1531, http://dx.doi.org/10.1212/WNL.0b013e318233b33d.

[23] K. Mevel, G. Chételat, F. Eustache, B. Desgranges, The default mode network in healthy aging and Alzheimer's disease, Int. J. Alzheimer's Dis. 2011 (2011) 1–9, http://dx.doi.org/10.4061/2011/535816.

[24] G. Simic, M. Babic, F. Borovecki, P.R. Hof, Early failure of the default-mode network and the pathogenesis of Alzheimer's disease, CNS Neurosci. Ther. 20 (7) (2014) 692–698, http://dx.doi.org/10.1111/cns.12260.

[25] C. Babiloni, X. Arakaki, H. Azami, K. Bennys, K. Blinowska, L. Bonanni, A. Bujan, M.C. Carrillo, A. Cichocki, J. Frutos-Lucas, C. Del Percio, B. Dubois, R. Edelmayer, G. Egan, S. Epelbaum, J. Escudero, A. Evans, F. Farina, K. Fargo, A. Fernández, R. Ferri, G. Frisoni, H. Hampel, M.G. Harrington, V. Jelic, J. Jeong, Y. Jiang, M. Kaminski, V. Kavcic, K. Kilborn, S. Kumar, A. Lam, L. Lim, R. Lizio, D. Lopez, S. Lopez, B. Lucey, F. Maestú, W.J. McGeown, I. McKeith, D.V. Moretti, F. Nobili, G. Noce, J. Olichney, M. Onofrj, R. Osorio, M. Parra-Rodriguez, T. Rajji, P. Ritter, A. Soricelli, F. Stocchi, I. Tarnanas, J.P. Taylor, S. Teipel, F. Tucci, M. Valdes-Sosa, P. Valdes-Sosa, M. Weiergräber, G. Yener, B. Guntekin, Measures of resting state EEG rhythms for clinical trials in Alzheimer's disease: Recommendations of an expert panel, Alzheimer' s Dement. 17 (9) (2021) 1528–1553, http://dx.doi.org/10.1002/alz.12311.

[26] J. Jeong, EEG dynamics in patients with Alzheimer's disease, Clin. Neurophysiol. 115 (7) (2004) 1490–1505, http://dx.doi.org/10.1016/j.clinph.2004.01.001.

[27] F. Vecchio, C. Babiloni, R. Lizio, F. De Vico Fallani, K. Blinowska, G. Verrienti, G. Frisoni, P.M. Rossini, Resting state cortical EEG rhythms in Alzheimer's

disease, in: Supplements To Clinical Neurophysiology, Vol. 62, Suppl Clin Neurophysiol, 2013, pp. 223–236, http://dx.doi.org/10.1016/B978-0-7020-5307-8.00015-6.

[28] U. Smailovic, V. Jelic, Neurophysiological markers of Alzheimer's disease: Quantitative EEG approach, Neurol. Ther. 8 (S2) (2019) 37–55, http://dx.doi.org/10.1007/s40120-019-00169-0.

[29] M. Şeker, Y. Özbek, G. Yener, M.S. Özerdem, Complexity of EEG dynamics for early diagnosis of Alzheimer's disease using permutation entropy neuromarker, Comput. Methods Programs Biomed. 206 (2021) 106116, http://dx.doi.org/10.1016/j.cmpb.2021.106116.

[30] C.T. Briels, D.N. Schoonhoven, C.J. Stam, H. de Waal, P. Scheltens, A.A. Gouw, Reproducibility of EEG functional connectivity in Alzheimer's disease, Alzheimer' s Res. Ther. 12 (1) (2020) 68, http://dx.doi.org/10.1186/s13195-020-00632-3.

[31] M.M. Engels, C.J. Stam, W.M. van der Flier, P. Scheltens, H. de Waal, E.C. van Straaten, Declining functional connectivity and changing hub locations in Alzheimer's disease: an EEG study, BMC Neurol. 15 (1) (2015) 145, http://dx.doi.org/10.1186/s12883-015-0400-7.

[32] P. Núñez, J. Poza, C. Gómez, V. Rodríguez-González, A. Hillebrand, M.A. Tola-Arribas, M. Cano, R. Hornero, Characterizing the fluctuations of dynamic resting-state electrophysiological functional connectivity: reduced neuronal coupling variability in mild cognitive impairment and dementia due to Alzheimer's disease, J. Neural Eng. 16 (5) (2019) 056030, http://dx.doi.org/10.1088/1741-2552/ab234b.

[33] G.C. O'Neill, E.L. Barratt, B.A.E. Hunt, P.K. Tewarie, M.J. Brookes, Measuring electrophysiological connectivity by power envelope correlation: a technical review on MEG methods, Phys. Med. Biol. 60 (21) (2015) R271–R295, http://dx.doi.org/10.1088/0031-9155/60/21/R271.

[34] B.J. Roach, D.H. Mathalon, Event-related EEG time-frequency analysis: An overview of measures and an analysis of early Gamma band phase locking in schizophrenia, Schizophr. Bull. 34 (5) (2008) 907–926, http://dx.doi.org/10.1093/schbul/sbn093.

[35] P. Tass, M.G. Rosenblum, J. Weule, J. Kurths, A. Pikovsky, J. Volkmann, A. Schnitzler, H.-J. Freund, Detection of m:n phase locking from noisy data: Application to magnetoencephalography, Phys. Rev. Lett. 81 (1998) 3291–3294, http://dx.doi.org/10.1103/PhysRevLett.81.3291.

[36] C.J. Stam, G. Nolte, A. Daffertshofer, Phase lag index: Assessment of functional connectivity from multi channel EEG and MEG with diminished bias from common sources, Hum. Brain Mapp. 28 (11) (2007) 1178–1193, http://dx.doi.org/10.1002/hbm.20346.

[37] S. Kasakawa, T. Yamanishi, T. Takahashi, K. Ueno, M. Kikuchi, H. Nishimura, Approaches of phase lag index to EEG signals in Alzheimer's disease from complex network analysis, in: Smart Innovation, Systems and Technologies, Vol. 45, Springer Science and Business Media Deutschland GmbH, 2016, pp. 459–468, http://dx.doi.org/10.1007/978-3-319-23024-5_42.

[38] H. Yu, X. Wu, L. Cai, B. Deng, J. Wang, Modulation of spectral power and functional connectivity in human brain by acupuncture stimulation, IEEE Trans. Neural Syst. Rehabil. Eng. 26 (2018) 977–986, http://dx.doi.org/10.1109/TNSRE.2018.2828143.

[39] H. Yu, X. Li, X. Lei, J. Wang, Modulation effect of acupuncture on functional brain networks and classification of its manipulation with EEG signals, IEEE Trans. Neural Syst. Rehabil. Eng. 27 (2019) 1973–1984, http://dx.doi.org/10.1109/TNSRE.2019.2939655.

[40] W. de Haan, Y.A. Pijnenburg, R.L. Strijers, Y. van der Made, W.M. van der Flier, P. Scheltens, C.J. Stam, Functional neural network analysis in frontotemporal dementia and alzheimer's disease using EEG and graph theory, BMC Neurosci. 10 (1) (2009) 1–12, http://dx.doi.org/10.1186/1471-2202-10-101/FIGURES/6.

[41] C.A. Frantzidis, A.B. Vivas, A. Tsolaki, M.A. Klados, M. Tsolaki, P.D. Bamidis, Functional disorganization of small-world brain networks in mild Alzheimer's disease and amnestic mild cognitive impairment: an EEG study using relative wavelet entropy (RWE), Front. Aging Neurosci. 6 (AUG) (2014) 224, http://dx.doi.org/10.3389/fnagi.2014.00224.

[42] C. Stam, B. Jones, G. Nolte, M. Breakspear, P. Scheltens, Small-world networks and functional connectivity in Alzheimer's disease, Cerebral Cortex 17 (1) (2006) 92–99, http://dx.doi.org/10.1093/cercor/bhj127.

[43] F.C. Morabito, M. Campolo, D. Labate, G. Morabito, L. Bonanno, A. Bramanti, S. de Salvo, A. Marra, P. Bramanti, A longitudinal EEG study of Alzheimer's disease progression based on a complex network approach, Int. J. Neural Syst. 25 (02) (2015) 1550005, http://dx.doi.org/10.1142/S0129065715500057.

[44] R. Wang, Z. Yang, J. Wang, L. Shi, An improved visibility graph analysis of EEG signals of Alzheimer brain, in: 2018 11th International Congress on Image and Signal Processing, BioMedical Engineering and Informatics, CISP-BMEI, IEEE, 2018, pp. 1–5, http://dx.doi.org/10.1109/CISP-BMEI.2018.8633052.

[45] H. Yu, X. Lei, Z. Song, C. Liu, J. Wang, Supervised network-based fuzzy learning of EEG signals for Alzheimer's disease identification, IEEE Trans. Fuzzy Syst. 28 (2020) 60–71, http://dx.doi.org/10.1109/TFUZZ.2019.2903753.

[46] A.L. Bokde, M. Ewers, H. Hampel, Assessing neuronal networks: Understanding Alzheimer's disease, Prog. Neurobiol. 89 (2) (2009) 125–133, http://dx.doi.org/10.1016/j.pneurobio.2009.06.004.

[47] M. Yu, O. Sporns, A.J. Saykin, The human connectome in Alzheimer disease — relationship to biomarkers and genetics, Nat. Rev. Neurol. 17 (9) (2021) 545–563, http://dx.doi.org/10.1038/s41582-021-00529-1.

[48] T. Demiralp, Z. Bayraktaroglu, D. Lenz, S. Junge, N.A. Busch, B. Maess, M. Ergen, C.S. Herrmann, Gamma amplitudes are coupled to theta phase in human EEG during visual perception, Int. J. Psychophysiol. 64 (1) (2007) 24–30, http://dx.doi.org/10.1016/j.ijpsycho.2006.07.005.

[49] A. Morillas-Romero, M. Tortella-Feliu, X. Bornas, P. Putman, Spontaneous EEG theta/beta ratio and delta–beta coupling in relation to attentional network functioning and self-reported attentional control, Cogn. Affect. Behav. Neurosci. 15 (3) (2015) 598–606, http://dx.doi.org/10.3758/s13415-015-0351-x.

[50] J.P. Trammell, P.G. MacRae, G. Davis, D. Bergstedt, A.E. Anderson, The relationship of cognitive performance and the theta-alpha power ratio is age-dependent: An EEG study of short term memory and reasoning during task and resting-state in healthy Young and old adults, Front. Aging Neurosci. 9 (NOV) (2017) 364, http://dx.doi.org/10.3389/fnagi.2017.00364.

[51] M.J. Brookes, P.K. Tewarie, B.A. Hunt, S.E. Robson, L.E. Gascoyne, E.B. Liddle, P.F. Liddle, P.G. Morris, A multi-layer network approach to MEG connectivity analysis, NeuroImage 132 (2016) 425–438, http://dx.doi.org/10.1016/j.neuroimage.2016.02.045.

[52] P. Tewarie, A. Hillebrand, B.W. van Dijk, C.J. Stam, G.C. O'Neill, P. Van Mieghem, J.M. Meier, M.W. Woolrich, P.G. Morris, M.J. Brookes, Integrating cross-frequency and within band functional networks in resting-state MEG: A multi-layer network approach, NeuroImage 142 (2016) 324–336, http://dx.doi.org/10.1016/j.neuroimage.2016.07.057.

[53] L. Cai, X. Wei, J. Liu, L. Zhu, J. Wang, B. Deng, H. Yu, R. Wang, Functional integration and segregation in multiplex brain networks for Alzheimer's disease, Front. Neurosci. 14 (2020) 51, http://dx.doi.org/10.3389/FNINS.2020.00051.

[54] A. Naro, M.G. Maggio, A. Leo, R.S. Calabrò, Multiplex and multilayer network EEG analyses: A novel strategy in the differential diagnosis of patients with chronic disorders of consciousness, Int. J. Neural Syst. 31 (02) (2021) 2050052, http://dx.doi.org/10.1142/S0129065720500525.

[55] S.J. Ruiz-Gómez, R. Hornero, J. Poza, E. Santamaría-Vázquez, V. Rodríguez-González, A. Maturana-Candelas, C. Gómez, A new method to build multiplex networks using canonical correlation analysis for the characterization of the Alzheimer's disease continuum, J. Neural Eng. 18 (2) (2021) 026002, http://dx.doi.org/10.1088/1741-2552/abd82c.

[56] J. Guillon, Y. Attal, O. Colliot, V. La Corte, B. Dubois, D. Schwartz, M. Chavez, F. De Vico Fallani, Loss of brain inter-frequency hubs in Alzheimer's disease, Sci. Rep. 7 (1) (2017) 10879, http://dx.doi.org/10.1038/s41598-017-07846-w, arXiv:1701.00096.

[57] M. Yu, M.M.A. Engels, A. Hillebrand, E.C.W. van Straaten, A.A. Gouw, C. Teunissen, W.M. van der Flier, P. Scheltens, C.J. Stam, Selective impairment of hippocampus and posterior hub areas in alzheimer's disease: an MEG-based multiplex network study, Brain 140 (5) (2017) 1466–1485, http://dx.doi.org/10.1093/brain/awx050.

[58] G.M. McKhann, D.S. Knopman, H. Chertkow, B.T. Hyman, C.R. Jack, C.H. Kawas, W.E. Klunk, W.J. Koroshetz, J.J. Manly, R. Mayeux, R.C. Mohs, J.C. Morris, M.N. Rossor, P. Scheltens, M.C. Carrillo, B. Thies, S. Weintraub, C.H. Phelps, The diagnosis of dementia due to Alzheimer's disease: Recommendations from the National Institute on Aging-Alzheimer's Association workgroups on diagnostic guidelines for Alzheimer's disease, Alzheimer' s Dement. 7 (3) (2011) 263–269, http://dx.doi.org/10.1016/j.jalz.2011.03.005.

[59] M.F. Folstein, S.E. Folstein, P.R. McHugh, "Mini-mental status". a practical method for grading the cognitive state of patients for the clinician, J. Psychiatr. Res. 12 (3) (1975) 189–198, http://dx.doi.org/10.1016/0022-3956(75)90026-6.

[60] C.A. Anderson, F.H. Pettersson, G.M. Clarke, L.R. Cardon, A.P. Morris, K.T. Zondervan, Data quality control in genetic case-control association studies, Nat. Protoc. 5 (9) (2010) 1564–1573, http://dx.doi.org/10.1038/nprot.2010.116.

[61] S. Purcell, B. Neale, K. Todd-Brown, L. Thomas, M.A. Ferreira, D. Bender, J. Maller, P. Sklar, P.I. de Bakker, M.J. Daly, P.C. Sham, PLINK: A tool set for whole-genome association and population-based linkage analyses, Am. J. Hum. Genet. 81 (3) (2007) 559–575, http://dx.doi.org/10.1086/519795.

[62] P.D. Sundar, C.-E. Yu, W. Sieh, E. Steinbart, R.M. Garruto, K. Oyanagi, U.-K. Craig, T.D. Bird, E.M. Wijsman, D.R. Galasko, G.D. Schellenberg, Two sites in the MAPT region confer genetic risk for Guam ALS/PDC and dementia, Hum. Mol. Gen. 16 (3) (2007) 295–306, http://dx.doi.org/10.1093/hmg/ddl463.

[63] A. Myers, M. Kaleem, L. Marlowe, A. Pittman, A. Lees, H. Fung, J. Duckworth, D. Leung, A. Gibson, C. Morris, R. de Silva, J. Hardy, The H1c haplotype at the MAPT locus is associated with Alzheimer's disease, Hum. Mol. Gen. 14 (16) (2005) 2399–2404, http://dx.doi.org/10.1093/hmg/ddi241.

[64] Y. Compta, M. Ezquerra, E. Muñoz, E. Tolosa, F. Valldeoriola, J. Rios, A. Cámara, M. Fernández, M.T. Buongiorno, M.J. Marti, High cerebrospinal tau levels are associated with the rs242557 tau gene variant and low cerebrospinal β-amyloid in Parkinson disease, Neurosci. Lett. 487 (2) (2011) 169–173, http://dx.doi.org/10.1016/j.neulet.2010.10.015.

[65] L. Fidani, K. Kalinderi, S. Bostantjopoulou, J. Clarimon, A. Goulas, Z. Katsarou, J. Hardy, A. Kotsis, Association of the Tau haplotype with Parkinson's disease in the Greek population, Mov. Disorders 21 (7) (2006) 1036–1039, http://dx.doi.org/10.1002/mds.20864.

[66] L.S. Elias-Sonnenschein, S. Helisalmi, T. Natunen, A. Hall, T. Paajanen, S.-K. Herukka, M. Laitinen, A.M. Remes, A.M. Koivisto, K.M. Mattila, T. Lehtimäki, F.R.J. Verhey, P.J. Visser, H. Soininen, M. Hiltunen, Genetic loci associated with Alzheimer's disease and cerebrospinal fluid biomarkers in a finnish case-control cohort, in: P. Lewis (Ed.), PLoS ONE 8 (4) (2013) e59676, http://dx.doi.org/10.1371/journal.pone.0059676.

[67] G. Das, A.K. Misra, S.K. Das, K. Ray, J. Ray, Microtubule-associated protein tau (MAPT) influences the risk of Parkinson's disease among Indians, Neurosci. Lett. 460 (1) (2009) 16–20, http://dx.doi.org/10.1016/j.neulet.2009.05.031.

[68] M. Allen, M. Kachadoorian, Z. Quicksall, F. Zou, H. Chai, C. Younkin, J.E. Crook, V. Pankratz, M.M. Carrasquillo, S. Krishnan, T. Nguyen, L. Ma, K. Malphrus, S. Lincoln, G. Bisceglio, C.P. Kolbert, J. Jen, S. Mukherjee, J.K. Kauwe, P.K. Crane, J.L. Haines, R. Mayeux, M.A. Pericak-Vance, L.A. Farrer, G.D. Schellenberg, J.E. Parisi, R.C. Petersen, N.R. Graff-Radford, D.W. Dickson, S.G. Younkin, N. Ertekin-Taner, Association of MAPT haplotypes with Alzheimer's disease risk and MAPT brain gene expression levels, Alzheimer' s Res. Ther. 6 (4) (2014) 39, http://dx.doi.org/10.1186/alzrt268.

[69] C. Wider, C. Vilariño-Güell, B. Jasinska-Myga, M.G. Heckman, A.I. Soto-Ortolaza, S.A. Cobb, J.O. Aasly, J.M. Gibson, T. Lynch, R.J. Uitti, Z.K. Wszolek, M.J. Farrer, O.A. Ross, Association of the MAPT locus with Parkinson's disease, Eur. J. Neurol. 17 (3) (2010) 483–486, http://dx.doi.org/10.1111/j.1468-1331.2009.02847.x.

[70] M.J. Machiela, S.J. Chanock, Ldlink: a web-based application for exploring population-specific haplotype structure and linking correlated alleles of possible functional variants: Fig. 1., Bioinformatics 31 (21) (2015) 3555–3557, http://dx.doi.org/10.1093/bioinformatics/btv402.

[71] A. Maturana-Candelas, C. Gómez, J. Poza, N. Pinto, R. Hornero, EEG characterization of the Alzheimer's disease continuum by means of multiscale entropies, Entropy 21 (6) (2019) 544, http://dx.doi.org/10.3390/e21060544.

[72] A. Maturana-Candelas, C. Gómez, J. Poza, S.J. Ruiz-Gómez, R. Hornero, Inter-band bispectral analysis of EEG background activity to characterize Alzheimer's disease continuum, Front. Comput. Neurosci. 14 (2020) 70, http://dx.doi.org/10.3389/fncom.2020.00070.

[73] S. Ruiz-Gómez, C. Gómez, J. Poza, G. Gutiérrez-Tobal, M. Tola-Arribas, M. Cano, R. Hornero, Automated multiclass classification of spontaneous EEG activity in Alzheimer's disease and mild cognitive impairment, Entropy 20 (1) (2018) 35, http://dx.doi.org/10.3390/e20010035.

[74] R.D. Pascual-Marqui, Standardized low-resolution brain electromagnetic tomography (sLORETA): technical details, Methods Find. Exp. Clin. Pharmacol. 24 Suppl D (2002) 5–12.

[75] B.T.T. Yeo, F.M. Krienen, J. Sepulcre, M.R. Sabuncu, D. Lashkari, M. Hollinshead, J.L. Roffman, J.W. Smoller, L. Zöllei, J.R. Polimeni, B. Fischl, H. Liu, R.L. Buckner, The organization of the human cerebral cortex estimated by intrinsic functional connectivity, J. Neurophysiol. 106 (3) (2011) 1125–1165, http://dx.doi.org/10.1152/jn.00338.2011.

[76] S. Palva, J.M. Palva, Discovering oscillatory interaction networks with M/EEG: challenges and breakthroughs, Trends Cogn. Sci. 16 (4) (2012) 219–230, http://dx.doi.org/10.1016/j.tics.2012.02.004.

[77] J.-M. Schoffelen, J. Gross, Source connectivity analysis with MEG and EEG, Hum. Brain Mapp. 30 (6) (2009) 1857–1865, http://dx.doi.org/10.1002/hbm.20745.

[78] S.J. Ruiz-Gómez, R. Hornero, J. Poza, A. Maturana-Candelas, N. Pinto, C. Gómez, Computational modeling of the effects of EEG volume conduction on functional connectivity metrics. Application to Alzheimer's disease continuum, J. Neural Eng. 16 (6) (2019) 066019, http://dx.doi.org/10.1088/1741-2552/ab4024.

[79] F. Battiston, V. Nicosia, V. Latora, Structural measures for multiplex networks, Phys. Rev. E 89 (3) (2014) 032804, http://dx.doi.org/10.1103/PhysRevE.89.032804, arXiv:1308.3182.

[80] S. Achard, C. Delon-Martin, P.E. Vértes, F. Renard, M. Schenck, F. Schneider, C. Heinrich, S. Kremer, E.T. Bullmore, Hubs of brain functional networks are radically reorganized in comatose patients, Proc. Natl. Acad. Sci. 109 (50) (2012) 20608–20613, http://dx.doi.org/10.1073/pnas.1208933109.

[81] Y. Benjamini, Y. Hochberg, Controlling the false discovery rate: A practical and powerful approach to multiple testing, J. R. Stat. Soc. Ser. B Stat. Methodol. 57 (1) (1995) 289–300, http://dx.doi.org/10.1111/j.2517-6161.1995.tb02031.x.

[82] R. Vaz-Drago, N. Custódio, M. Carmo-Fonseca, Deep intronic mutations and human disease, Hum. Genet. 136 (9) (2017) 1093–1111, http://dx.doi.org/10.1007/s00439-017-1809-4.

[83] E. Majounie, W. Cross, V. Newsway, A. Dillman, J. Vandrovcova, C.M. Morris, M.A. Nalls, L. Ferrucci, M.J. Owen, M.C. O'Donovan, M.R. Cookson, A.B. Singleton, R. de Silva, H.R. Morris, Variation in tau isoform expression in different brain regions and disease states, Neurobiol. Aging 34 (7) (2013) 1922.e7–1922.e12, http://dx.doi.org/10.1016/j.neurobiolaging.2013.01.017.

[84] C. Beste, A. Münchau, C. Frings, Towards a systematization of brain oscillatory activity in actions, Commun. Biol. 6 (1) (2023) 137, http://dx.doi.org/10.1038/s42003-023-04531-9.

[85] H. Braak, K. Del-Tredici, C. Schultz, E. Braak, Vulnerability of select neuronal types to Alzheimer's disease, Ann. New York Acad. Sci. 924 (2000) 53–61, http://dx.doi.org/10.1111/j.1749-6632.2000.tb05560.x.

[86] A. Rubinski, N. Franzmeier, A. Dewenter, Y. Luan, R. Smith, O. Strandberg, R. Ossenkoppele, M. Dichgans, O. Hansson, M. Ewers, Higher levels of myelin are associated with higher resistance against tau pathology in Alzheimer's disease, Alzheimer' s Res. Ther. 14 (1) (2022) 139, http://dx.doi.org/10.1186/s13195-022-01074-9.

[87] D.C. Dean, S.A. Hurley, S.R. Kecskemeti, J.P. O'Grady, C. Canda, N.J. Davenport-Sis, C.M. Carlsson, H. Zetterberg, K. Blennow, S. Asthana, M.A. Sager, S.C. Johnson, A.L. Alexander, B.B. Bendlin, Association of amyloid pathology with Myelin alteration in preclinical Alzheimer disease, JAMA Neurol. 74 (1) (2017) 41–49, http://dx.doi.org/10.1001/JAMANEUROL.2016.3232.

[88] J.M. Kernbach, B.T. Thomas Yeo, J. Smallwood, D.S. Margulies, M.T. De Schotten, H. Walter, M.R. Sabuncu, A.J. Holmes, A. Gramfort, G. Varoquaux, B. Thirion, D. Bzdok, Subspecialization within default mode nodes characterized in 10,000 UK biobank participants, Proc. Natl. Acad. Sci. USA 115 (48) (2018) 12295–12300, http://dx.doi.org/10.1073/PNAS.1804876115/SUPPL_FILE/PNAS.1804876115.SAPP.PDF.

[89] X.T. Fang, T. Volpi, S.E. Holmes, I. Esterlis, R.E. Carson, P.D. Worhunsky, Linking resting-state network fluctuations with systems of coherent synaptic density: A multimodal fMRI and 11C-UCB-J PET study, Front. Hum. Neurosci. 17 (2023) 1124254, http://dx.doi.org/10.3389/fnhum.2023.1124254.

[90] M.V. Rockman, L. Kruglyak, Genetics of global gene expression, Nature Rev. Genet. 7 (11) (2006) 862–872, http://dx.doi.org/10.1038/nrg1964.

[91] E. Stomrud, O. Hansson, L. Minthon, K. Blennow, I. Rosén, E. Londos, Slowing of EEG correlates with CSF biomarkers and reduced cognitive speed in elderly with normal cognition over 4 years, Neurobiol. Aging 31 (2) (2010) 215–223, http://dx.doi.org/10.1016/j.neurobiolaging.2008.03.025.

[92] M. Das, S. Maeda, B. Hu, G.-Q. Yu, W. Guo, I. Lopez, X. Yu, C. Tai, X. Wang, L. Mucke, Neuronal levels and sequence of tau modulate the power of brain rhythms, Neurobiol. Dis. 117 (2018) 181–188, http://dx.doi.org/10.1016/j.nbd.2018.05.020.

[93] L. Canuet, S. Pusil, M.E. Lopez, R. Bajo, J.A. Pineda-Pardo, P. Cuesta, G. Galvez, J.M. Gaztelu, D. Lourido, G. Garcia-Ribas, F. Maestu, Network disruption and cerebrospinal fluid amyloid-beta and phospho-Tau levels in mild cognitive impairment, J. Neurosci. 35 (28) (2015) 10325–10330, http://dx.doi.org/10.1523/JNEUROSCI.0704-15.2015.

[94] U. Smailovic, T. Koenig, I. Kåreholt, T. Andersson, M.G. Kramberger, B. Winblad, V. Jelic, Quantitative EEG power and synchronization correlate with Alzheimer's disease CSF biomarkers, Neurobiol. Aging 63 (2018) 88–95, http://dx.doi.org/10.1016/j.neurobiolaging.2017.11.005.

[95] J.S.K. Kauwe, C. Cruchaga, K. Mayo, C. Fenoglio, S. Bertelsen, P. Nowotny, D. Galimberti, E. Scarpini, J.C. Morris, A.M. Fagan, D.M. Holtzman, A.M. Goate, Variation in MAPT is associated with cerebrospinal fluid tau levels in the presence of amyloid-beta deposition, Proc. Natl. Acad. Sci. 105 (23) (2008) 8050–8054, http://dx.doi.org/10.1073/pnas.0801227105.

[96] T. Ravid, M. Hochstrasser, Diversity of degradation signals in the ubiquitin–proteasome system, Nature Rev. Mol. Cell Biol. 9 (9) (2008) 679–689, http://dx.doi.org/10.1038/nrm2468.

[97] L.K. Rudenko, H. Wallrabe, A. Periasamy, K.H. Siller, Z. Svindrych, M.E. Seward, M.N. Best, G.S. Bloom, Intraneuronal Tau misfolding induced by extracellular amyloid-β oligomers, in: A. Alonso (Ed.), J. Alzheimer' s Dis. 71 (4) (2019) 1125–1138, http://dx.doi.org/10.3233/JAD-190226.

[98] S. Dujardin, S. Bégard, R. Caillierez, C. Lachaud, S. Carrier, S. Lieger, J.A. Gonzalez, V. Deramecourt, N. Déglon, C.-A. Maurage, M.P. Frosch, B.T. Hyman, M. Colin, L. Buée, Different tau species lead to heterogeneous tau pathology propagation and misfolding, Acta Neuropathol. Commun. 6 (1) (2018) 132, http://dx.doi.org/10.1186/s40478-018-0637-7.

[99] G.I. Hallinan, M. Vargas-Caballero, J. West, K. Deinhardt, Tau misfolding efficiently propagates between individual intact Hippocampal neurons, J. Neurosci. 39 (48) (2019) 9623–9632, http://dx.doi.org/10.1523/JNEUROSCI.1590-19.2019.

[100] N.I. Luna-Viramontes, B.B. Campa-Córdoba, M.Á. Ontiveros-Torres, C.R. Harrington, I. Villanueva-Fierro, P. Guadarrama-Ortíz, L. Garcés-Ramírez, F. de la Cruz, M. Hernandes-Alejandro, S. Martínez-Robles, E. González-Ballesteros, M. Pacheco-Herrero, J. Luna-Muñoz, PHF-core tau as the potential initiating event for Tau pathology in Alzheimer's disease, Front. Cell. Neurosci. 14 (2020) 247, http://dx.doi.org/10.3389/fncel.2020.00247.

[101] T. Fath, J. Eidenmüller, R. Brandt, Tau-mediated cytotoxicity in a pseudohyperphosphorylation model of Alzheimer's disease, J. Neurosci. 22 (22) (2002) 9733–9741, http://dx.doi.org/10.1523/JNEUROSCI.22-22-09733.2002.

[102] L. Troquier, R. Caillierez, S. Burnouf, F. J Fernandez-Gomez, M.-E. Grosjean, N. Zommer, N. Sergeant, S. Schraen-Maschke, D. Blum, L. Buee, Targeting phospho-ser422 by active tau immunotherapy in the THYTau22 mouse model: a suitable therapeutic approach, Curr. Alzheimer Res. 9 (4) (2012) 397–405.

[103] S. Jadhav, J. Avila, M. Schöll, G.G. Kovacs, E. Kövari, R. Skrabana, L.D. Evans, E. Kontsekova, B. Malawska, R. de Silva, L. Buee, N. Zilka, A walk through tau therapeutic strategies, Acta Neuropathol. Commun. 7 (2019) 22, http://dx.doi.org/10.1186/s40478-019-0664-z.

[104] N.E. Kadmiri, Tau-targeted immunotherapy for Alzheimer's disease: Insight into clinical trials, OBM Neurobiol. 08 (2024) 1–7, http://dx.doi.org/10.21926/obm.neurobiol.2403238.

[105] H. Yu, F. Li, J. Liu, D. Liu, H. Guo, J. Wang, G. Li, Evaluation of acupuncture efficacy in modulating brain activity with periodic-aperiodic EEG measurements, IEEE Trans. Neural Syst. Rehabil. Eng. 32 (2024) 2450–2459, http://dx.doi.org/10.1109/TNSRE.2024.3421648.